Holocene-long record of flood frequency in the Southern Alps (Lake Iseo, Italy) under human and climate forcing

William Rapuc, Pierre Sabatier, Fabien Arnaud, Antoine Palumbo, Anne-Lise Develle, ; Jean-Louis Reyss, Edouard Regnier, Andrea Piccin, Emmanuel Chapron, Jean-Pascal Dumoulin, et al.

Holocene-long record of flood frequency in the Southern Alps (Lake Iseo, Italy) under human and climate forcing

William Rapuc (1), Pierre Sabatier (1), Fabien Arnaud (1), Antoine Palumbo (1), Anne-Lise Develle (1), Jean-Louis Reyss (1), Laurent Augustin (2), Edouard Régnier (3), Andrea Piccin (4), Emmanuel Chapron (5), Jean-Pascal Dumoulin (3) and Ulrich von Grafenstein (3)

(1) Univ. Grenoble Alpes, Univ. Savoie Mont Blanc, CNRS, EDYTEM, 73000 Chambéry, France

(2) Division technique de l'INSU, Centre de Carottage et de Forage National, CNRS, France

(3) LSCE, Université de Versailles Saint-Quentin, Commissariat à l'Energie Atomique–CNRS, 91198 Gif-sur-Yvette, France

(4) Regione Lombardia, D.G. Territorio e Urbanistica, Struttura Sistema Informativo Territoriale, 20124 Milano, Italy

(5) Laboratoire GEODE, UMR 5602 CNRS-Université Toulouse Jean Jaurès, Maison de la Recherche, 31058 Toulouse, France

Abstract

A high-resolution sedimentological and geochemical analysis of a 21 m sediment sequence of Lake Iseo (Southern Alps, Italy) allowed for the reconstruction of the long-term flood frequency by visual identification of the event layers over the last 12 kyr cal BP. In a previous study that was undertaken on another sediment core from Lake Iseo, these layers were attributed to extreme surface runoff events. However, in this former core, large mass-wasting deposits that induce significant hiatuses did not permit a continuous record of flood events to be established. Such disturbances were absent in the core studied in the present paper. This permitted to establish a high-resolution continuous Holocene record. Based on the flood chronicle and sedimentological and XRF geochemical analyses,

we found evidence of a major palaeohydrological transition at approximately 3.8 kyr cal BP, which was previously described as occurring in the western Mediterranean region. The oldest part of the record indeed presents a very low frequency of flood events (< 1 flood/century), while after 4 kyr cal BP, the flood frequency increased. This pattern appears to be in agreement with other Southern Alpine paleo flood records. The transition is interpreted as a nonlinear climate response to the orbital-driven gradual decrease in summer insolation at 60°N, which together with the influence of the Mediterranean mesoscale precipitation events, is typical for the Mediterranean climate. However, the comparison of the flood record with the archaeological and historical data from the watershed suggests that human activity during the Roman period in the vicinity of the main tributaries also influenced the flood frequency. Even in a large Alpine lake and more than 2000 years ago, extreme precipitation events that were recorded through the sedimentation process can hence be impacted by the anthropization of the catchment area pointing the requirement of deeper studies of Earth surface critical zone pluri-millennial dynamics.

Keywords

Lake sediment; Holocene; Flood chronicle; Human impact; Southern Alps

1. Introduction

In mountainous areas, floods are among the most damaging climatic events in terms of economic and societal losses (Gaume et al., 2009; Glur et al., 2013). In the context of global climate changes, the intensification of catastrophic events, such as floods, is expected in European regions (Hirabayashi et al., 2013). Indeed, even if a decrease in summer precipitation is expected in the Alps by the year 2100, extreme precipitation events that are associated with convective rainfall are assumed to increase (Giorgi et al., 2016). However, tendencies at the regional and local scales are still uncertain, and the study of these extreme events represents a major issue for natural hazards

assessment (Stocker et al., 2013). The use of geological paleoclimate records is necessary to understand the past variations of these events in contrasting climatic contexts (Beniston et al., 2007). Lake sediments are widely used to reconstruct paleo-flood activity, as flood events are recorded in a long-term and continuous way (Bøe et al., 2016; Giguet-Covex et al., 2012; Gilli et al., 2013; Glur et al., 2013; Moreno et al., 2008; Noren et al., 2002; Wilhelm et al., 2012; Wirth et al., 2013).

In ideal conditions, paleo-flood records that are obtained from lake sediment can be used as a proxy of local or regional extreme paleo-hydrological patterns (Sabatier et al., 2017; Wilhelm et al., 2013; Wirth et al., 2013). In the context of an environment that is stressed by human activities, soil is more easily mobilized by precipitation events. Indeed, land-use and forest clearance generally increase soil erodibility and runoff efficiency (Brisset et al., 2017; Cosandey et al., 2005). Recently, several studies have shown that human activities in the small-size watershed could influence the frequency of floods that are recorded in mountain lake sediments (Brisset et al., 2017; Giguet-Covex et al., 2012). However, in a recent review, Arnaud et al., (2016) proposed that the influence of human activity upon geological record of erosive events should be minimal in a large lake fed by a large, diversified catchment area. To go a step further in discriminating climate and human impact on lake sediment-based flood chronicles, we propose here the study of a lowland lake fed by a medium-sized catchment area and located in a region where the long-term regional climate trend and human activity are well-documented.

We studied a sediment sequence from Lake Iseo at the downstream end of the Val Camonica valley in Northern Italy. Various paleoclimate records from this region already exist, which will be used to discuss the regional representativeness of our new flood chronicle (Magny et al., 2012, 2009; Vannière et al., 2013; Wirth et al., 2013). Human activities were also well-documented in the Val Camonica from the first settlements and in the first trace of agricultural practices that are dated to the Mesolithic (Anati and Cittadini, 1994) and the Neolithic periods (Gehrig, 1997), respectively. A high number of rock carvings and archaeological sites were discovered and studied in the Val Camonica

valley (Anati and Cittadini, 1994; Arcà and Fossati, 2006; Nash, 2011; Nash and Chippindale, 2002). Information about human activities along the shores of Lake Iseo are also accessible, including periods of human presence on the delta, the date of the creation of main Marone infrastructure as well as the age and location of archeological sites (Benedetti and Predali, 2013; Condina, 1986; Gregorini et al., 2012; Predali, 2013, 2010, 2008).

Here, we used a multi-proxy approach to combine the sedimentology and geochemistry to identify millimetric flood layers of a well-dated lake Iseo sediment sequence and, thus, to understand the long-term influence of human activities on the flood activity recorded in low elevation lake catchments in the alpine area.

2. Study Site and Geological Settings

Lake Iseo (45°44.205'N; 10°4.340'E) is a large lowland lake in Northern Italy, with a length of 25 km and a surface area of 60.9 km². This perialpine lake is located in Lombardy, north of the Po plain (**Fig. 1A**), at the southern-end of the Val Camonica valley at an altitude of 185 m above sea level (a.s.l). The depression that hosts the lake corresponds to a Miocene canyon that was reshaped and re-eroded by several glacier advances during the Pleistocene epoch (Bini et al., 1978). The main tributary and the unique outlet of Lake Iseo are part of the Oglio River, which has its headwaters in the Adamello massif in the Northern part of Val Camonica (**Fig. 1B**). This valley is known for a high number of rock carvings that are registered on the UNESCO World Heritage List, as they provide indications of human presence in the Iseo region since the Mesolithic (9000 – 6000 BC) period (Anati and Cittadini, 1994). Numerous archeological sites that are dated from the Camuni and Roman periods are also present around the Lake and in the southern-end of Val Camonica, north of Lake Iseo (Condina, 1986). In this region, the first trace of sparse agricultural activities was found in pollen records that date to approximately 7 kyr cal BP (Gehrig, 1997).

The bathymetric map highlights the presence of two basins in Lake Iseo separated by Monte Isola, which is the largest lake island in Italy (**Fig. 1B**). The main basin spreads West of Monte Isola and

presents a maximum water depth of 256 m below lake surface (b.l.s). East of Monte Isola, the lake morphology presents a shallower sub-basin (approximately 100 m deep) named Sale Marasino Basin. Northward, this basin is separated from Monte Isola Plateau (70 m b.l.s) by a 30-m-high escarpment. Monte Isola Plateau is isolated from the deeper basin by the 180-m-high Monte Isola Escarpment.

In terms of water supply, the Monte Isola Plateau (MIP) and the Sale Marasino Basin (SMB) are mainly fed by the Oglio River and small tributaries coming from the slopes, east of the Sale Marasino and Marone towns. MIP and SMB are located 11.4 km away from the Oglio inlet and are separated from the main basin by a 180-m-high escarpment (**Figs. 1B&C**). This difference in elevation appears to be important enough to prevent underflows or interflows from the Oglio River from reaching the Monte Isola Plateau. Moreover, under ordinary flow conditions and under higher a discharge rate, the Oglio river is deflected toward the western shore of the lake due to the Coriolis influence (Pilotti et al., 2018, 2013). The overflow plume is, thus, generally brought to the western shore of Lake Iseo (Pilotti et al., 2018) and is unlikely to influence the Monte Isola Plateau and the Sale Marasino Basin on the eastern shore.

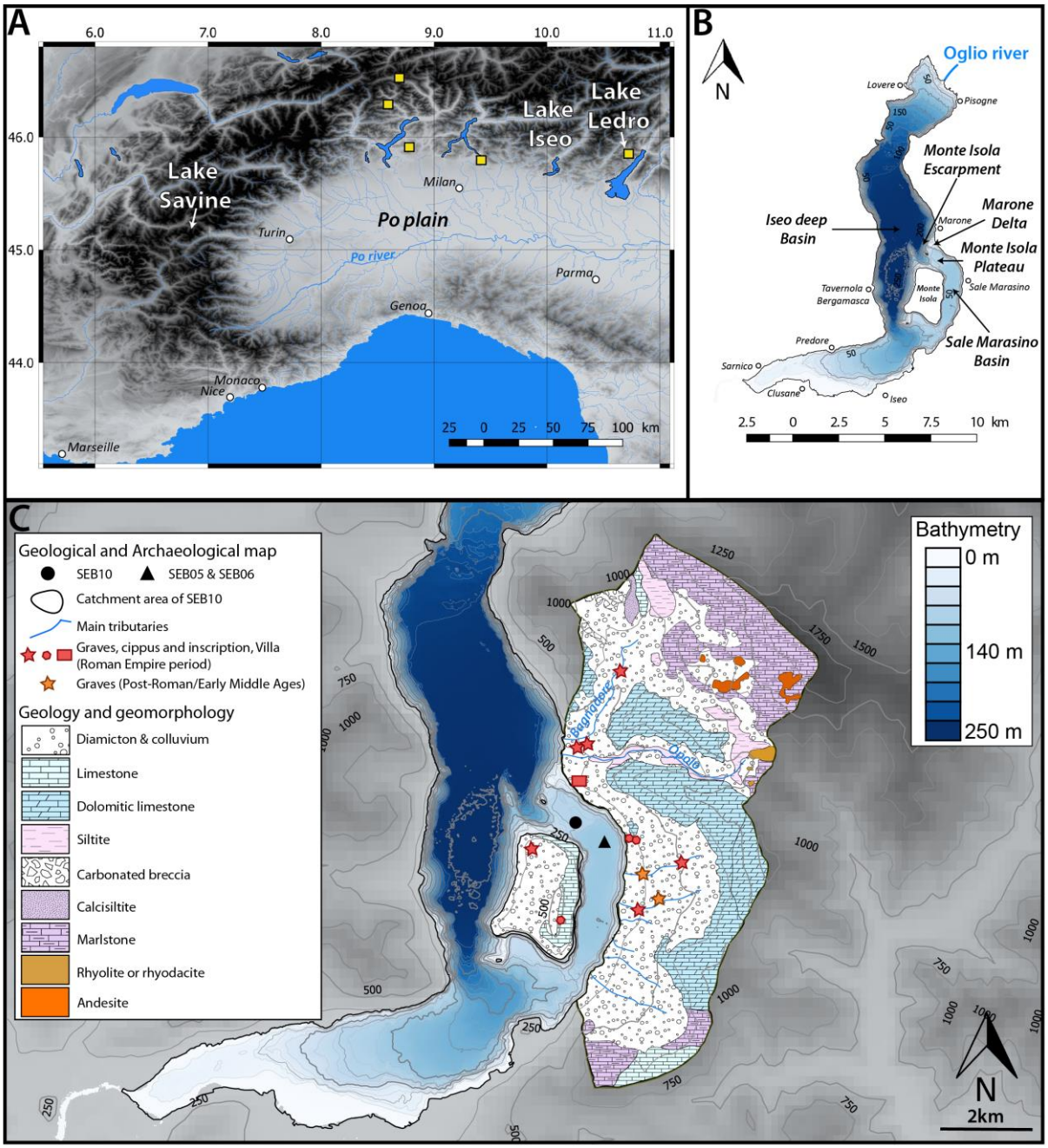

Figure 1 - Lake Iseo location and settings. (A) Locations of Lake Iseo (Italy) and the different lakes used hereafter for comparison: Lake Savine (France), Lake Ledro (Italy). The yellow squares correspond to the location of the different lakes that were used by Wirth et al., (2013) to construct a flood chronicle for the southern Alps. (B) Lake Iseo Bathymetric map associated with the description of the different morphological features and the main cities. (C) Geological map and archaeological sites of the watershed draining the *Marone and Sale Marasino* towns*.*

Therefore, in terms of the sediment supply, the catchment area of MIP and SMB is limited to the slopes East of the shores. This catchment is mainly drained by two tributaries: the Opolo and the Bagnadore torrents (**Fig. 1C**). The inlet of these two rivers is located in the Marone village, which is in the northern part of the MIP. Other small gullies are present on the mountain slopes East of Sale Marasino and on

Monte Isola, however, as a first approximation, we will consider the Opolo and Bagnadore as the main terrigenous sediment sources on our study site.

The watershed of MIP and SMB is mainly composed of Quaternary colluvium, which cover the valley bottoms and the lower part of the slopes around Sale Marasino and Marone. The Upper part of the catchment and the main summits are composed of a thick pile of Upper Triassic/Lower Jurassic dolomitic limestone (**Fig. 1C**). Triassic marlstones outcrops are present in the upper part of Opolo and Bagnadore river catchments and the southern-end of the catchment area. Jurassic limestones were also reported on Monte Isola and in the southeast part of the watershed. Few Andesite and Rhyolite outcrops are present in the upper part of the Opolo and Bagnadore catchment areas. These magmatic features that originated from the Upper Triassic tectonic collapse in the region were associated with normal faults (Buffoli, 2014; Presbitero et al., 2011).

3. Materials and Methods

3.1. Seismic Survey, Coring and Lithological Description

A high-resolution seismic reflection survey using a broad-band (300–2400 Hz) single-channel boomer device (Bini et al., 2007) was conducted on Lake Iseo in 2002. This survey was previously used to select a coring site in the Eastern sub-basin, which provided the first Holocene flood record (Lauterbach et al., 2012). However, a large mass-wasting deposit that induced an important hiatus prevented a continuous record from being established on those sequences. Therefore, a new seismic survey using a 3.5 kHz system and covering the MIP and SMB with a seismic network of shoreline-parallel and perpendicular transects with approximately 200 m distance was conducted in 2007 (data already included in Lauterbach et al., 2012). This helped to select a new coring site on Monte Isola plateau between Monte Isola and Marone (45° 43.312'N; 10° 5.771'E) at an approximately 70-m-water depth, in which earthquake-induced mass-wasting deposits were absent. In 2010, 23.2-m-long sediment sections from three holes in close vicinity were retrieved from the lake by using a 90-mm diameter piston corer on a Uwitec coring platform (EDYTEM/LSCE/C2FN). All sections were split, photographed

at high resolution (20 pixels.mm^{-1}), described and logged in detail using the Munsell color chart. The identification of specific layers on the overlapping sections allowed us to construct a 21.4-m-long composite sediment sequence (hereafter called SEB10).

3.2. Grain-size Analysis

We performed grain-size analyses on 425 samples throughout the uppermost 10 meters on the SEB10 sediment core. Samples were chosen from continuous sedimentation and interbedded deposits. The analyses were conducted under sonicate but without any chemical pretreatment at the EDYTEM laboratory using a Malvern MasterSizer S™ (Malvern Instruments Ltd) with a grainsize range between 0.06 µm and 800 µm. Hereafter, we will use, the median (Q50) and the coarsest fraction (Q90), among other factors, to characterize all of the sedimentary layers. In order to characterize the deposit energy of instantaneous deposits thicker than 5mm, we will use the Q90max, i.e. the highest Q90 of the whole sequence (Wilhelm et al., 2013).

3.3. Loss on Ignition (LOI)

A 10-cm evenly spaced discrete sampling step was applied on the uppermost 10 meters of the SEB10 sequence to perform Loss on Ignition following the protocol that was defined by Heiri et al., (2001). The detrital layers were not included in the collected samples. This analysis was conducted to quantify the organic matter and carbonate content throughout the sediment sequence. Before the LOI analysis, the dry bulk density (DBD) was calculated from the same sediment samples by performing a constant volume sampling and weighing the sediment after 72 h of drying at 60°C. Then, the sediment samples were first dried and crushed before being heated in an oven at 550°C for 4 h and at 950°C for 2 h. The relative weight loss during the first (hereafter, LOI550°C) and second heating phases (hereafter, LOI950°C) corresponds to the fractions of organic matter and of carbonate, respectively.

3.4. Geochemical Properties

To characterize the variations of major elements throughout SEB10 sediment sequence, we performed X-ray fluorescence (XRF) geochemical analyses on the EDYTEM laboratory's AVAATECH Core Scanner

(Avaatech XRF Technology). A continuous 5-mm step measurement was applied with a run at 10 kV and 0.3 mA for 30 s to detect lightweight elements, such as Al, Si, K, Ca, Ti, Mn, and Fe, and a second run was performed at 30 kV and 0.4 mA for 40 s to detect Br, Rb, Sr and Zr. The XRF core scanning results are expressed hereafter as peak intensities counting (cps). Then, a principle component analysis (PCA) was conducted on the XRF data to identify principal sediment end-members and correlations between the detected elements (Sabatier et al., 2010).

3.5. Dating

On the SEB10 sediment sequence, we combined short-lived radionuclides (^{210}Pb, ^{137}Cs, ^{241}Am), varve counting and ^{14}C to build a precise age-depth model of the uppermost 12.65 meters. The first 40 cm of the sequence was sampled with a 1-cm sampling step to measure short-lived radionuclide contents at the Laboratoire Souterrain de Modane using the well-type germanium detectors (Reyss et al., 1995). Thirty-two samples of vegetal macro-organic remains were used to perform ^{14}C measurements at the LMC14 laboratory (CNRS). Dates were calibrated at 2 sigma using the Intcal13 calibration curve (Reimer et al., 2013), and the age-depth model was performed using the R code package “clam” in R software (Blaauw, 2010).

4. RESULTS

4.1. Sedimentology

4.1.1. Sedimentary units

Along the 21.4 m of the SEB10 sedimentary sequence, six different units from the top to the bottom of the core were observed and described (**Fig. 2**). As this study focuses on the Holocene time scale, only the first 12 m of the sequence will be described here, as the deepest 10 m correspond to Late glacial deposits, which is confirmed hereafter by age-depth modeling (**see section 4.2.2**).

Unit 1 (0-19 cm) is composed of dark-greenish-gray clay (5GY 4/4) that presents a thin alternation of dark green, light gray and gray laminae on the first 19 cm of the core. This unit matches with the one

that was described first by Lauterbach et al., (2012) and was identified as an organic gyttja that corresponds to the recent eutrophication period of lake Iseo. The values of LOI550°C vary between 9 to 11 % with a mean value of 10.7 %, while LOI950°C values range between 17.3 and 15.5 % with a mean value of 16.3 %. Across this unit, we count 53 laminae successions. From 19 cm to 1057.5 cm, the SEB10 core is mainly composed of gray clay frequently interbedded by thin dark-brown clay-to-silty layers. This section was subdivided into four different units according to the color variations from the top to the bottom of the record (**Fig. 2**). Unit IIa (19-276.6 cm) presents olive-gray clay (5Y/5/2) that becomes slightly lighter. The LOI550°C results range between 6.4 to 9.3 %, with a mean value of 7.3 %, and the LOI 950°C results in this unit range between 3.5 to 14.2 % with a mean value of 8.2 %. Unit IIb (276.6-596.8 cm) is light-olive-gray and presents more frequent intercalation of dark-brown clay-to-silty layers. This unit presents a lower LOI550°C mean value of 6.3 %, with values ranging from 4.9 to 7.5 % and a higher 10.6 % LOI950°C mean value, with values ranging from 4.6 to 14.4 %. Unit IIc (596.8-925 cm) is light-gray and slightly bluish (5 GY 7/1) and is composed of an alternation of beige and dark clayey laminae. This unit presents values of LOI550°C ranging between 5.2 to 8.2 % with a mean value of 6.3 %, and the values of LOI950°C range between 3.7 and 15.6 % with a mean value of 8.2 %. Unit IId (925-1057.5 cm) is composed of gray (2.5Y/6/1) clay showing pale-yellow, reddish-yellow and olive-gray color alternations with very few silty layers and laminae. In this unit, the LOI550°C results range between 5.7 and 7.4 % with a mean value of 6.2 %, and the LOI950°C results range between 3 to 10.5 % with a mean value of 8.1 %. Unit III (1057.5-1187.5 cm) is defined as a gray clay unit (5Y/5/1) wherein the sediment becomes lighter without silty layers with very few organic debris, and it presents beige-orange laminated sections (**Fig. 2**).

4.1.2. Geochemistry analyses

From the XRF analyses, Unit I shows low values of Ti [>10,000 counts per second (cps)] and K (>45,000 cps) and high values of Ca (> 250,000 cps). From the top of the sediment section to Unit III, the Ti and K signals increase. The Br signal is constant over the first 12 m of the SEB10 sediment core, except for

several peaks that correspond to specific deposits. The Ca signal is highly variable but does not allow a distinction between the different units.

The Br and Ca contents that were obtained from the XRF analyses were combined to the LOI results in linear regression tests. The relationship between the LOI950°C and the Ca content is positive, with an R^2 of 0.54 (p-value < 3.1×10^{-18}), which suggests that the Ca content could be used as a high-resolution proxy of carbonate. In the literature, the Br content is usually a proxy of organic matter (Bajard et al., 2016); nevertheless, here, the relationship with LOI550°C is poorly constrained with a positive R^2 of 0.14 (p-value > 0.56).

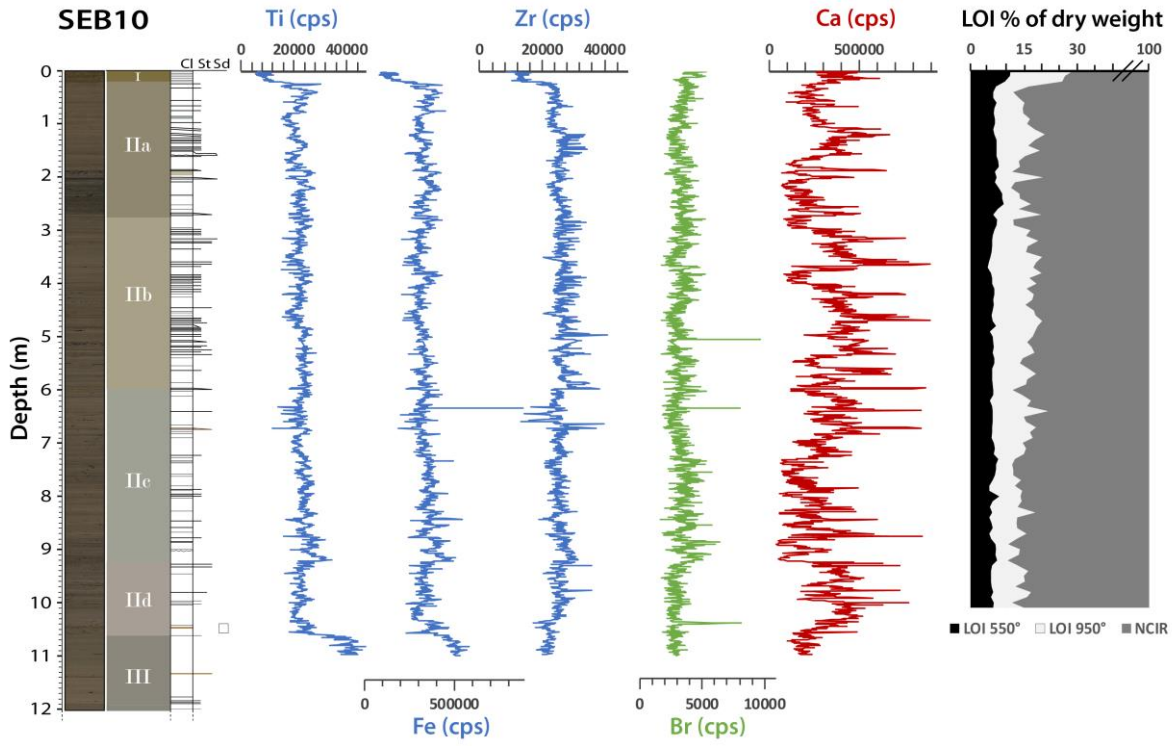

Figure 2 - Main sedimentological and geochemical results. A picture of the first 12 m of the SEB10 sediment sequence is associated with the lithological description (with corresponding units named I, IIa, IIb, IIc, IId and III), geochemical results (Ti, Fe, Zr, Br, and Ca contents) and Loss on Ignition (LOI).

A principal component analysis was conducted on the XRF data and provides variables and individual factor maps (**Fig. 3**), which highlight the relationships between the different elements and the geochemical distribution within sediment units. Dimensions 1 and 2 (denoted as Dim1 and Dim2) represent 62.3 % of the total variability. From the variables factor map, three end-members were identified. The first one, which is denoted as terrigenous, is positively correlated with Dim1 and yields

high positive loadings for the major terrigenous elements (Al, Si, K, Ti, Rb, Fe). The second one, which is denoted as “organic matter” yields positive values for Br and is negatively correlated with Dim2. However, as the Br signal is poorly correlated with LOI550°C, this end-member will not be used hereafter. The third one is negatively correlated with Dim1 and is positively correlated with Dim2. This pole yields high positive values for Ca and Sr and is, thus, interpreted as representative of the carbonates input from the watershed, as Sr is usually present in marine limestone, which constitutes a major part of the watershed outcrops. The Individuals factor map (**Fig. 3**) highlights the specificity of each unit: (i) Unit I is negatively correlated with terrigenous end-members, which is due to its high organic matter (LOI550° > 11 %, Lauterbach et al., 2012) and carbonate (LOI950°C > 17 %) contents. (ii) Unit III is positively correlated with Dim1 and, thus, to the detrital end-member, and it is also characterized by low Ca and Sr contents. (iii) Unit IIa, IIb, IIc and IId are not well distinguishable from this map, but there is a decreasing trend of the contents of terrigenous elements, which is clearly visible from Unit III to Unit II.

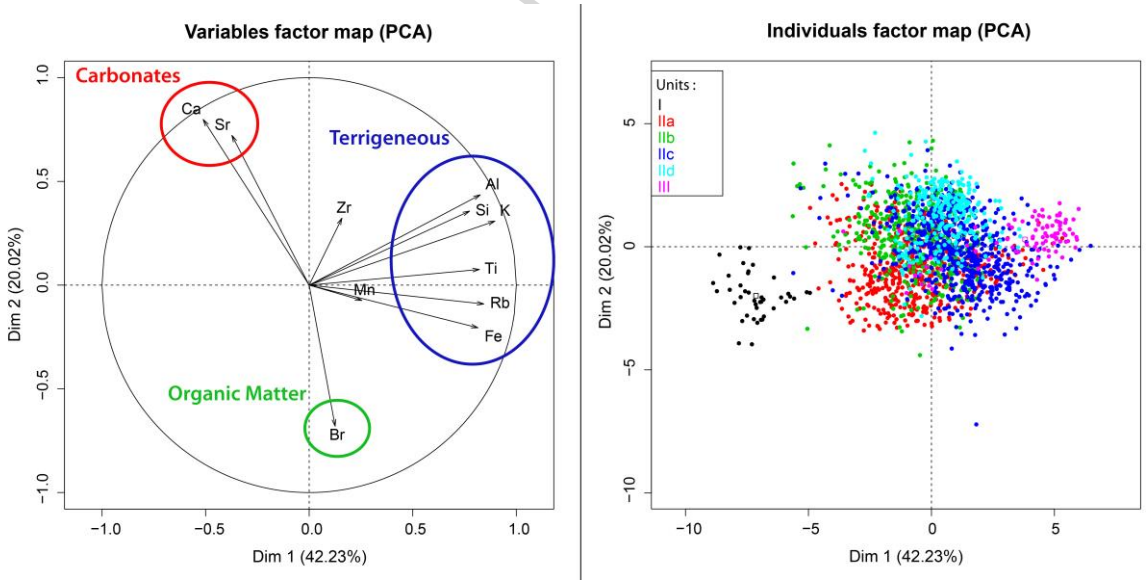

Figure 3 - Variable and Individual factor maps from the PCA. (A) Variable factor map with three endmembers (terrigenous, organic matter and carbonates). (B) Individual factor map with sedimentological units added as an illustrative variable.

4.1.3. Graded beds

Several layers that are clearly distinguishable from the normal sedimentation by their colors and textures were observed along the sedimentary sequence. The first type of deposits, which are denoted

hereafter as Type 1 (T1), correspond to thin millimetric to centimetric dark-brown deposits with a silty base. These deposits are very similar to the detrital layers that were observed on the Sale Marasino plateau sediment sequence by Lauterbach et al., (2012).

When T1 layers were thicker than the 5mm sampling step (49 over 148), it was possible to individually characterize both their grainsize and geochemical fingerprint. In those deposits $Q90_{max}$ values are between 20 and 80 µm and vary from 60 at the base to 20 µm at the top of a random graded bed, and median values ($Q50_{max}$) are between 3 to 10 µm (**Fig. 4**) and Zr/Fe ratio and Mn present a peak at the base of each sequence. In order to verify the attribution of thinner-than-5mm visually-determined layers to the T1 deposit type, we lowered the sampling step down to 1mm on a 50cm-long core section (Fig. 4). This confirmed the presence of a peak in Mn in each of the layers in agreement with the observation made on thicker ones. The Zr/Fe peak was not systematically observed, however a relative enrichment in Zr or Fe was evidenced for each layer, as marked by Zr/Ti and Fe/Ti ratio, respectively. Based on those observations, we decided to classify all of the 148 brown deposits identified from the background sedimentation by a visual lithological description as T1 deposits. The majority (91 on 148 deposits) of these T1 deposits were observed in Unit IIb (276.6-596.8 cm), whereas very few were counted in Units IIc, IId and III. The T1 deposits range between 1 and 41 mm with a mean size of 5.8 mm.

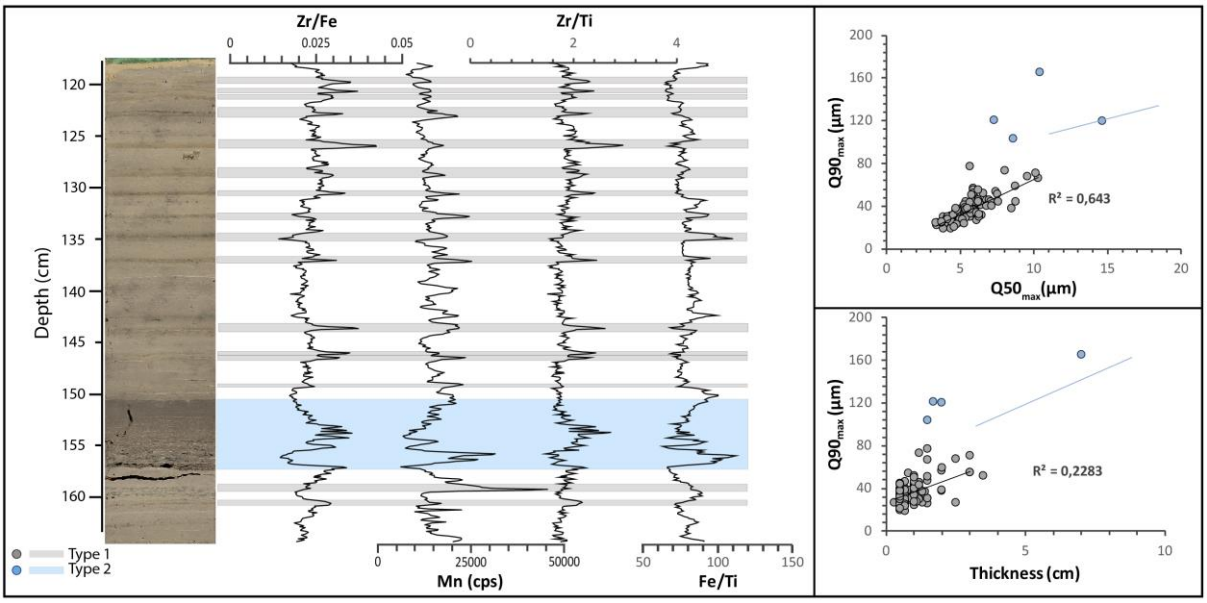

Figure 4 - Detailed results for the two types of graded layers that were observed in the SEB10 sequence. The left panel presents the SEB10-02A picture according to the master core depth in cm associated with the Zr/Fe, Mn, Zr/Ti and Fe/Ti signals that were derived from the XRF-CS analysis at 1 mm resolution. The Type 1 layers (T1) are highlighted in gray, while T2 are highlighted in blue. The upper-right panel presents the relation between Q90max (the highest Q90 value of each graded-bed) and the median (Q50max) expressed in µm. The lower-right panel presents the relation between Q90max and the thickness of each deposit. The coefficient of determinations were calculated for the T1 deposits.

Four other deposits were also identified in the SEB10 sediment sequence and will be denoted as Type 2 deposits (T2) hereafter. T2 deposits present a mean thickness of 47 mm and are, thus, comparatively thicker than T1 deposits (mean thickness of 5.8 mm). Based on a grain-size analysis and the relationship between $Q90_{max}$ and $Q50_{max}$, they are coarser than T1 with relatively higher $Q90_{max}$ (>100 µm) (**Fig. 4**). The base of these deposits is made of to coarse silt and to fine sand. They are also less well sorted than T1 (mean sorting of 3.9 for T2 compared to 2.9 for T1). The proportion of silt and sand progressively decreases from the bottom to the top. The T2 deposits are, thus, normally graded beds. The Zr/Fe and Mn signals also present peaks in the T2 layers, but the signals are more complex within the base of these deposits (**Fig. 4**). The T2 layer that is presented in Fig. 4 shows low values of Zr/Fe, followed by peaks in the middle of the deposit. Several peaks of the Mn signal are also observable. These four T2 layers could be interpreted as thicker and coarser expressions of the T1 layers. However, the differences in the grain size and in the XRF signals could be important enough to be related to a difference in the triggering mechanisms and lead us to distinguish between these two types of deposits which we however attribute to instantaneous deposits.

4.2. Chronology

4.2.1. Short-lived radionuclides

The ^{210}Pb excess profile ($^{210}Pb_{ex}$) profile shows a regular decrease (**Fig. 5A**) from 400 mBq.g^{-1} to low activities (<50 mBq.g^{-1}). Here, we use a logarithmic scale to plot these data and to underscore a well-constrained single-point alignment that shows a constant sedimentation rate of 3.12±0.06 mm yr^{-1} (R^2=0.97) for the uppermost 30 cm, for which the most superficial sample showed very low $^{210}Pb_{ex}$ and was not considered. The ^{137}Cs profile shows a clear peak between 4.8 and 7.3 cm with a maximum activity (>1300 mBq.g^{-1}) at 7.3 cm; this peak is associated with a peak of ^{241}Am (>3 mBq.g-^{1}) and is widely attributed in the literature to nuclear fallout from the 1986 Chernobyl accident (e.g., Appleby et al., 1991). The ^{241}Am profile presents a peak (>3 mBq.g^{-1}) between 13 and 15 cm with moderate ^{137}Cs activity and a first increase at 17 cm. These two depths correspond to the maximum nuclear weapon tests at AD 1963 at 13.5 cm and with the first appearance of ^{137}Cs dated to AD 1955 (Appleby et al., 1991). These two peaks are in good agreement with the sedimentation rate that was derived from the $^{210}Pb_{ex}$ profile.

Fifty varves were identified and counted from the top of the sediment section to 15 cm, which provides a 3 mm yr^{-1} sedimentation rate that is highly comparable with the rate that was derived from the CFCS model and ^{137}Cs and ^{241}Am profiles (**Fig. 5A**). The first varve was dated at 1960 AD and could correspond to the beginning of the lake eutrophication (Jenny et al., 2013), which is quite identical to the timing that was observed in Lake Varese in Northern Italy (Bruel et al., 2018), where both climatic and anthropogenic impacts played a role into lake anoxia.

Thus, we added these chronological data into the age-depth model to constrain it for the upper portion of the sedimentary record (**Fig. 5B**).

4.2.2. ^{14}C & Age-depth model

Twenty-seven samples of terrestrial macroremains were analyzed to provide a radiocarbon age. After calibration, 3 of these 27 samples (**Table 1**) presented ages that were too old to fit the SEB10 age-

depth model, which was probably linked to the reworking of old material (**Fig. 5B**). The first outlier was sampled at 21.5 cm and was too old compared to the $^{210}Pb_{excess}$ profile that was obtained at that depth (**Fig. 5B**). Both the second and third outliers are present within a group of other radiocarbon dates and emerge slightly from the trend of their respective groups due to old age. Thus, they were rejected from the model to avoid reversals and inconsistencies (**Fig. 5B**). The two kinds of graded layers that were previously described have been interpreted as instantaneous deposits, and the sum of their depths represent 104.5 cm for the first 12 m of the sediment sequence. To provide the best age-depth model, an event-free depth was created by subtracting all of the thicknesses of the instantaneous deposits from the SEB10 sequence sediment depth (Arnaud et al., 2002). The age-depth model was generated with the remaining 24 calibrated ages and the short-lived radionuclide ages. The best fit was obtained with the R code package "clam" (Blaauw, 2010) by applying a smooth spline model with 0.42 for the smooth parameter. The sedimentation rate presented hereafter was calculated without event layers. Finally, we reintegrated all instantaneous events to the age-depth model (**Fig. 5B**) to provide a date for all instantaneous deposits.

The first 10.5 m of SEB10 sequence covers the last ≈12, 000 years (**Fig. 5B**) with a mean sedimentation rate of 1 mm yr^{-1}. The sedimentation rate over this sequence varies from 3.23 to 0.39 mm yr^{-1}, with several peaks (Fig. 6A). From 12 to 8.7 kyr cal BP, the sedimentation rate is quite constant and varies between 0.6 to 0.4 mm yr^{-1}. A first increase is observed (**Fig. 5B**) from 8.7 kyr cal BP until a maximum rate of 0.81 mm yr^{-1} at 6.5 kyr cal BP is reached. The sedimentation rate then decreases until 5 kyr cal BP, with a minimum of 0.63 mm yr^{-1}. From 5 to 1 kyr cal BP, the sedimentation rate is highly variable and presents two maxima: one at 3.8 kyr cal BP with 1.48 mm yr^{-1} and one at 3 kyr cal BP with 1.58 mm yr^{-1}. This second increase follows directly after a period of decrease between 3.8 to 3.3 kyr cal BP, with a minimum rate of 1.17 mm yr^{-1}. From 3 kyr cal BP, the sedimentation rate decreases slightly until 1 kyr cal BP (0.94 mm yr^{-1}). Finally, the sedimentation rate increases to the top of the SEB10 sequence with a maximum rate of 3.21 mm yr^{-1} in 1960 AD.

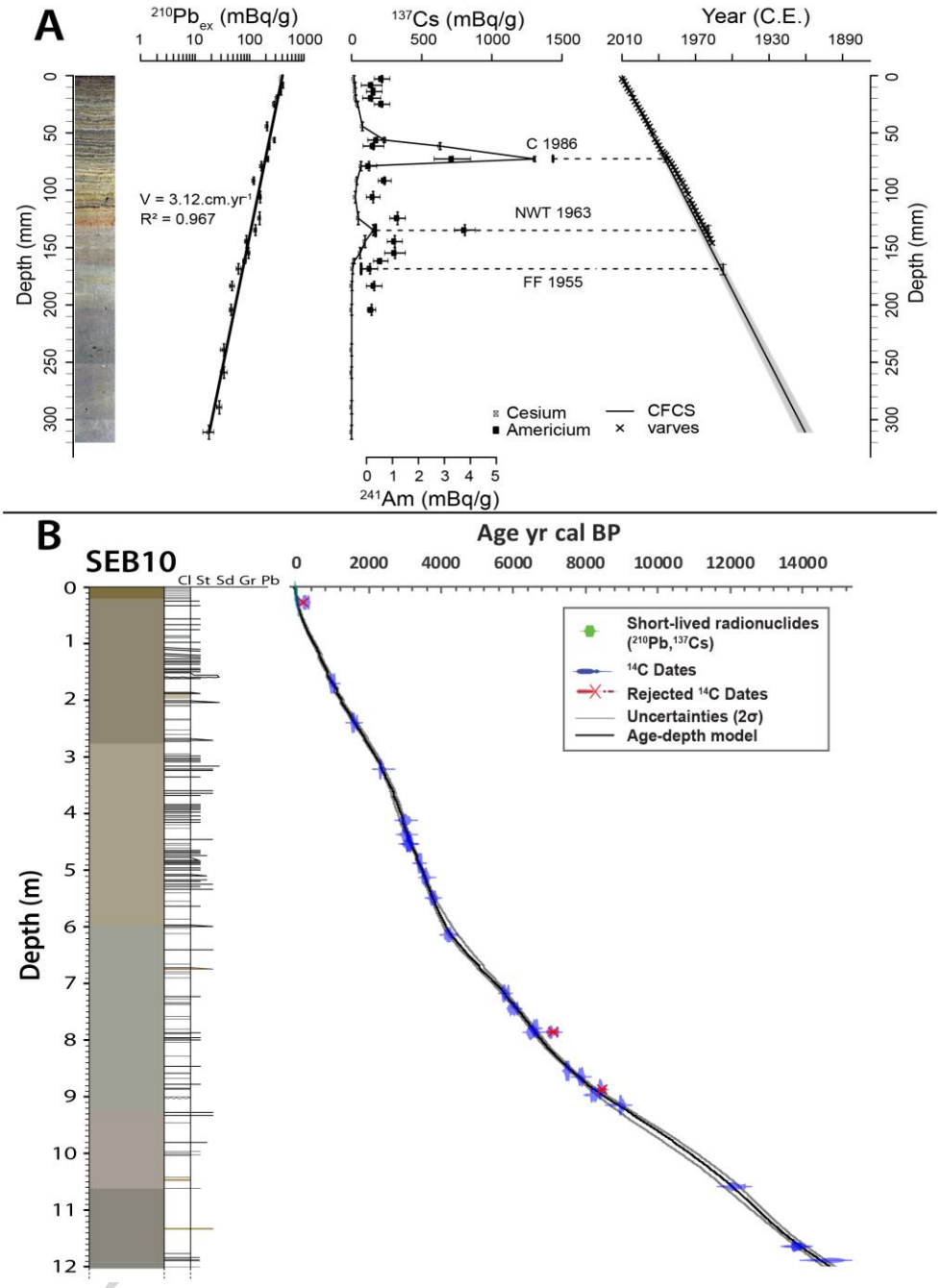

Figure 5 - Age-depth models. (A) Short-lived radionuclide data: $^{210}Pb_{ex}$ in logarithmic scale associated with the ^{241}Am and ^{137}Cs profiles with the picture of the top 35 cm of SEB10 sequence. (B) Age-depth model associating radiocarbon and short-lived radionuclide dates.

5. Discussion

5.1. Instantaneous deposits

The two kinds of detrital layers that were identified visually are graded beds, which are rich in angular allochthonous carbonates and silicates and present a silty to sandy base. Those are characteristic

features of flood-triggered deposits (Sturm and Matter, 1978). To better understand those deposits and their origins, we used the 1 mm XRF resolution between 120 and 165 cm of the SEB10 Mastercore (**Fig. 4**). As described previously, several T1 deposits present a peak of Zr/Fe and Mn at their base. The Zr/Fe ratio is linked to grain-size variations within the deposits: Zr is generally yielded by heavy minerals, while Fe is linked to aluminum silicates or oxides. A peak of the Zr/Fe ratio is, thus, expected to correspond to a coarser grain-size, which is generally attributed to a flood origin for underflow deposits (Wilhelm et al., 2013). A high Mn content in lake sediment could be linked to an oxygenation of the lake-sediment interface, by which Mn-Ca carbonates and Mn oxides can precipitate at the oxic/anoxic transition (Elbaz-Poulichet et al., 2014). When a flood occurs, the oxygen-rich water that is brought by the underflow reaches the lake water's-sediment interface and is conducted to the Mn precipitation. Thus, a peak of Mn can be interpreted as flood-induced lake bottom oxygenation and is linked to a detrital input (Sabatier et al., 2017). From **Fig. 4,** it appears that the T1 deposits did not always present a Zr/Fe peak but rather sometimes present a depletion of Zr/Fe. This could be due to the lateral variability of the geochemical composition of a turbidite (Bertrand et al., 2012). Indeed, if the analyzed layer corresponds to the distal or the proximal part of a turbidite, the composition will vary according to the principle that heavy or large minerals, such as zircons, will be deposited closer to the delta than will lightweight minerals, such as clay or oxides that are rich in Fe. Depending on the intensity of the underflow, the Zr/Fe ratio signal will then vary at the coring site. However, this can be solved by using a proxy of terrigenous input, which is supposed to be constant and not segregated laterally during flood deposits; one such proxy is Ti because it is yielded by Ti-oxides as well as by most of the silicates by substitution of Al. Then, plotting Zr/Ti and Fe/Ti was used to identify all the underflows (**Fig. 4**): a distal part of a turbidite will be enriched in Fe compared to Ti, whereas a proximal part of a turbidite will be enriched in Zr compared to Ti. Moreover, all of the T1 deposits present a peak of Mn signal at their base (**Fig. 4**), which reflects the fact that they are all linked to sediment input from underflows, which oxygenated the lake floor (Sabatier et al., 2017). The combination of Zr/Fe, Zr/Ti, Fe/Ti and Mn peaks at the base of the T1 deposits led us to interpret these underflow layers as

flood-triggered deposits. This interpretation is reinforced by the location of the coring site: the SEB10 sediment sequence is located on Monte Isola Plateau, where it avoids any slides from the escarpments. This interpretation is also in line with the previous work of Lauterbach et al., (2012) which observed and interpreted similar type of deposit as flood-triggered deposits on Sale Marasino plateau based on sediment microfacies, sediment lightness and magnetic susceptibility. The floods recorded here are linked to the sediment inputs from Opolo and Bagnadore streams and from few gullies from the watershed.

T2 deposits present coarser grain size values and are thicker compared to T1. They are also generally thinner for the same $Q90_{max}$ values and present higher sorting values. Zr/Fe and Mn signals show multiple peaks within the base of those layers. The Zr/Fe peaks imply a weaker sorting in the base of those layers. The presence of Mn peaks allows for the possibility that a delta collapse or a slide from the slopes are less probable, as the Mn peaks imply an oxygen-rich water input during the deposition. Thus, T2 deposits could be interpreted as a more proximal record of an underflow. However, the T2 deposit that is identified at 153 cm is dated at 865 ± 46 yr cal BP and could correspond to a slide that was induced by the same seismic event as that which produced the E1 large scale mass-wasting deposit that was identified by Lauterbach et al. (2012) in the SEB06 core and was dated at 759 ± 62 yr cal BP. Then, it is still unclear if those layers correspond to a single flood-input or a slide from previously deposited sediment on the Marone delta. Thus, we decided to remove them from the flood-chronicle that is presented hereafter. As there are only four T2 deposits, their absence does not have a significant impact on this chronicle.

From the last 12,000 years of the sedimentary record of the SEB10 sequence, 148 floods were identified visually and were dated through the T1 deposits to build a flood chronicle.

5.2. Flood chronicle

A flood chronicle was built and presents the variation of the number of floods that were recorded in the SEB10 sedimentary sequence per 100 years. In addition, the siliciclastic terrigenous flux (SCTF; g

cm^{-2} yr^{-1}) was calculated in order to link the flood chronicle and the evolution of erosion processes in the catchment area. SCTF was computed as the product of the % of non-carbonate ignition residue (NCIR), derived from the LOI analyses, and the sedimentation rate and the sediment density. The NCIR represents more than 80 % of the total sedimentation; thus, the SCTF could be interpreted as the total terrigenous flux. This flux depends on the sedimentation rate that is calculated without instantaneous deposits and thus represents the long-term detrital inputs from the watershed that will be used here as a proxy of erosion (Fig. 6A). Several different periods of can be distinguished from the flood chronicle and the SCTF (**Fig. 6B**):

(i) The sedimentation on the MIP before 12 kyr cal BP (Unit III) corresponds to Lateglacial deposits (LGD) according to the high values of detrital elements (Fig. 2).

(ii) The transition between LGD and the Holocene is marked by a decrease in detrital input from 12. Between 12 and 4.2 kyr cal BP (Unit IId & IIc), the sedimentation rate was low; very few floods were recorded on the SEB10 sediment sequence. At that time, the erosion in the watershed is low which can be due to the early development of Holocene soils just after the glaciers retreat (Bajard et al., 2016). Between 8.2 and 5.5 kyr cal BP (Unit IIc) the SCTF shows a slight increase, possibly due to a rise in erosion in the watershed.

(iii) From 4.2 to 2.1 kyr cal BP (Unit IIb), the erosion in the watershed increases sharply, according to the SCTF that reaches its highest value at 3.8 kyr cal BP. This peak is simultaneous with the outset of an increase in flood frequency (3.8 kyr cal BP). Between 3.8 and 2.9 kyr cal BP, the flood frequency signal varied intensely with peaks at 3.6, 3.3 and 2.9 kyr cal BP (**Fig. 6B**).

(iv) According to SCTF and the flood chronicle, the intensity of the erosion in the watershed decreases between 2.1 and 0.4 kyr cal BP (Unit IIa). Only one peak of high flood frequency is observable between 0.73 and 0.63 kyr cal BP (1220–1320 AD). From 0.4 kyr cal BP, the SCTF and the sedimentation rate defer from the flood chronicle and attested an increase of the erosion in the watershed.

(v) During the last 50 years (Unit I), the sedimentation processes change and varves appear probably due to the beginning of the Lake Eutrophication.

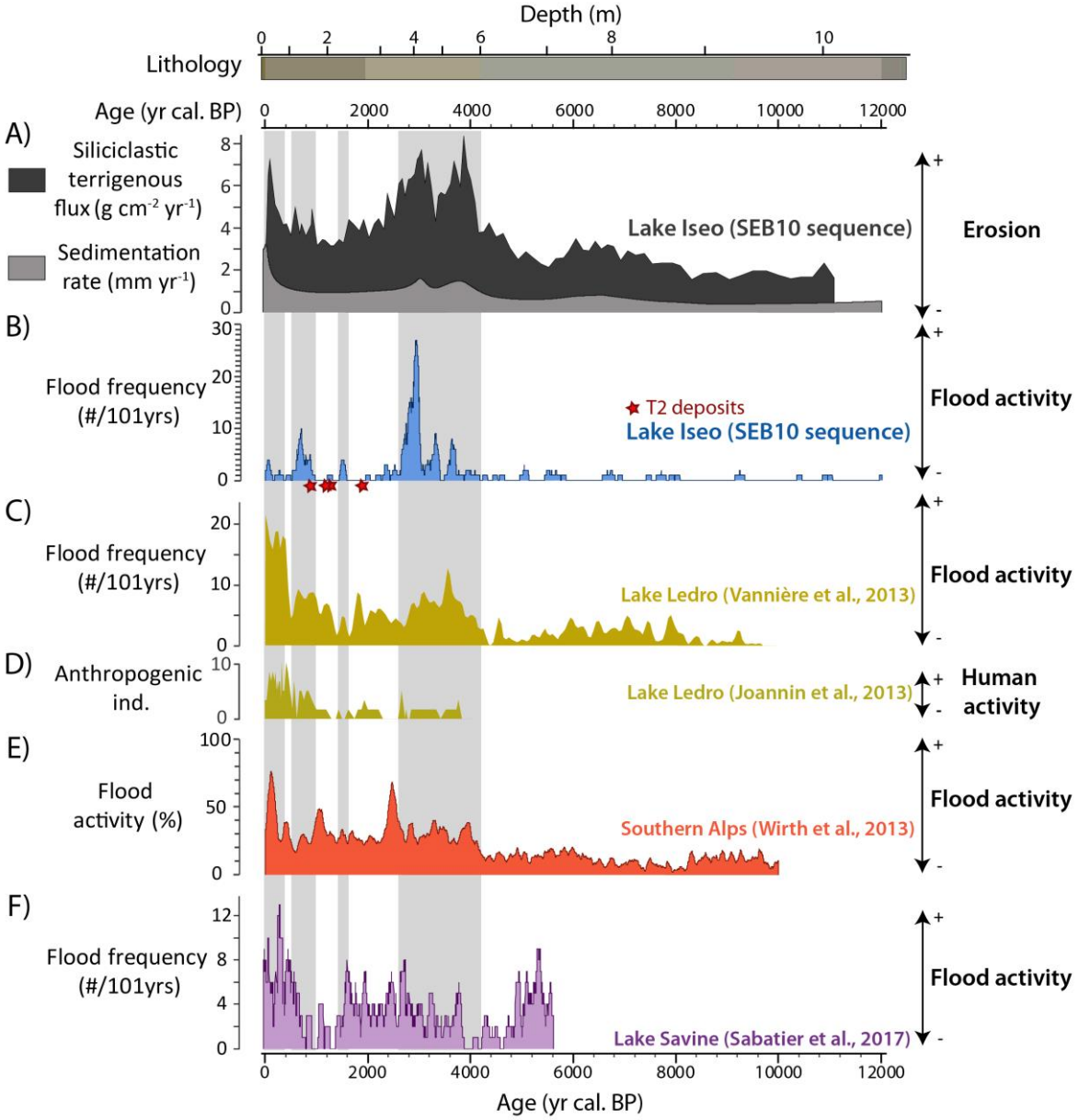

Figure 6 - Comparison between (A) SEB10 sedimentation rate and terrigenous flux with (B) SEB10 flood frequency and T2 deposits ages (red stars), (C) Lake Ledro flood activity and (D) Anthropogenic indicator (Joannin et al., 2013; Vannière et al., 2013), (E) the Southern Alps flood chronicle(Wirth et al., 2013) and (F) Lake Savine flood activity (Sabatier et al., 2017). Gray shadings highlights the periods of high erosion recorded in Lake Iseo.

In addition, peaks of high detrital flux on the SEB06 sediment core are also documented during high flood frequency periods of the SEB10 flood chronicle between 4.2 and 3.5 kyr cal BP and between 3 and 2.8 kyr cal BP (Lauterbach et al., 2012).

In the Alps, regardless of human influences, the flood frequency is generally higher during periods of cold and wetter climate, and vice versa (Czymzik et al., 2013; Giguet-Covex et al., 2012; Swierczynski et al., 2013; Wilhelm et al., 2012; Wirth et al., 2013). Moreover, lowland lakes, such as Lake Iseo, are less influenced by flash flood events and are generally more sensitive to long rain-triggered floods with a large spatial extent (Arnaud et al., 2016; Czymzik et al., 2013; Swierczynski et al., 2013). The floods that are chronicled from the SEB10 sequence are, thus, supposed to be first influenced by regional climate variation.

The period between 12 kyr and 4.2 kyr cal BP of the SEB10 flood chronicle is identical to other records from the Italian Alps, with low flood activity and low erosion (Vannière et al., 2013; Wirth et al., 2013; **Fig. 6B, C & E**). This time range is known as a stable warm and dry climate period in the Alps, in particular during the Holocene Climatic Optimum (9 to 5 kyr cal BP). Even if the human activity started in Italy and in the Val Camonica with the first settlements during the Mesolithic and the development of land use from the Early Neolithic (Rottoli and Castiglioni, 2009), no archaeological sites from these periods were discovered around Marone and Sale Marasino. Moreover, the Lake Ledro (653 m a.s.l) pollen record (Joannin et al., 2013; **Fig. 6D**) presents no anthropogenic indicators of that time.

From 4.2 kyr cal BP, the SCTF starts to increase until a peak at 3.8 kyr cal BP. The SCTF serves as a proxy of the erosion in the watershed. SCTF could be dominated by both long-term weak-to-medium intensity regional precipitation trends and changes in the vegetal cover, land use and multiple other factors linked to human activity (Bajard et al., 2017a, 2017b). Between 4.2 and 3.8 kyr cal BP, the anthropogenic indicator index of Lake Ledro, which is the closest anthropogenic record in the region, shows no human impact (Joannin et al., 2013). The long-term increase of the SCTF at that period is, thus, supposed to be linked to a transition toward regionally wetter climate conditions (Isola et al., 2019). Here, the increase of the SCTF is synchronous with the increases that were observed on other Alpine Lakes flood chronicles (**Fig. 6C, E & F**). This trend is also broadly observable in Northern Atlantic regions and is generally considered to be a nonlinear response to the progressive decrease of summer

insolation at 60°N (Magny et al., 2013). This change in the insolation pattern induced a switch toward a wetter and colder climate in Southern Europe and was linked to a more negative NAO and a southward migration of the Westerlies, thus producing an increase in the precipitation in the Southern Alps (Wirth et al., 2013). This trend was also observed for the Lake Savine flood chronicle in the French Alps (**Fig. 6F**), which presents the same shift toward higher flood frequency with a delay of 300 years (Sabatier et al., 2017). This small gap could be linked to both age-depth model uncertainties and to the more northern position of this lake.

From 3.8 kyr cal BP and the peak of SCTF, the flood frequency that was recorded for the SEB10 sequence starts to increase. This lag between the SCTF and the increase in the SEB10 flood frequency is possibly due to passing a critical threshold of precipitation intensity and/or erosion in the watershed, thus leading to the deposition of detrital layers onto the lake floor. The peaks of flood frequency on the SEB10 sediment sequence at 3.3 kyr and 2.9 kyr cal BP are synchronous with periods of high lake levels at Lake Ledro (Magny et al., 2009). However, the period from 3.6 kyr cal BP to 2.7 kyr cal BP is also known as a period of intense human activities in the Southern Alps with: (i) attested forest opening in the Swiss Alps (Dapples et al., 2002) and (ii) forest opening and an increase of the land use in the Lake Ledro watershed (Joannin et al., 2014; Vannière et al., 2013). Nevertheless, no archaeological sites from this period were discovered in the Marone watershed. By being part of a regional trend, the increase of the erosion in the watershed at 4.2 kyr cal BP seems to be driven by regional climatic conditions and is linked to a transition toward a wetter climate, with an increase in the influence of Mediterranean mesoscale precipitation events (Sabatier et al., 2017). However, if the extreme values that were observed in the flood chronicle at 3.3 and 2.9 kyr cal BP can be explained by a regionally more humid climate (Magny et al., 2009), it is doubtless that human activities by forest opening and land-use has favored soil erosion and, thus, influenced the record of flood activity at that time (Brisset et al., 2017; Giguet-Covex et al., 2012).

From 2.5 kyr cal BP, the flood chronicle seems disconnected from other flood chronicles and regional trends (**Figs. 6 & 7A**). Between 2.1 and 1.6 kyr cal BP (150 BC – 350 AD), no flood events were recorded in the SEB10 sediment sequence, although this period coincides with the Roman Empire period, which is characterized both by intense land-use and high flood frequency in geological records of lakes Ledro and Savine (**Figs. 6C, F**) and relatively high SCTF values in the SEB10 sequence (3.9 g cm^{-2} yr^{-1} on average between 2 and 1.5 kyr cal BP). The lack of recorded floods could be explained by a modification of the courses of Opolo and Bagnadore streams. This could be due to natural avulsion after an important flood event or by artificial embankment on the eastern shores of Lake Iseo (**Figs. 7B&C**). Indeed, a Roman Villa was occupied until almost 311 AD, and several graves were discovered close to the current location of the Marone village center (**Fig. 7B** Condina, 1986). The location of those archeological sites (**Fig. 7B**) suggests that the Marone Delta was occupied during Roman times, which led to a possible modification of the Opolo and Bagnadore torrents courses to prevent avulsions (**Fig. 7B**). Thus, the Opolo and Bagnadore streams were probably flowing into Lake Iseo in the northern part of the Marone delta at that time. When the stream confluences are located North of the Marone delta, there was no possible sediment input on Monte Isola Plateau, as the sediment is directly thrown into the Lake Iseo deeper basin (**Fig. 7B**). To justify this statement, it should be pointed out that two historical flood events almost entirely damaged Marone village in 1953 and 1963, bringing huge amounts of sediment from Opolo and Bagnadore watersheds (Benedetti and Predali, 2013) but did not lead to detrital deposits in our Monte Isola Plateau sediment core. From the 16th century, Opolo and Bagnadore streams were dammed in the center of Marone, and their flows were connected to the northern part of the Marone delta (Predali, 2013, 2008). According to the bathymetric map, only the Marone delta developed on the MIP, which means that the natural courses of Opolo and Bagnadore streams were located on the southern part of the delta.

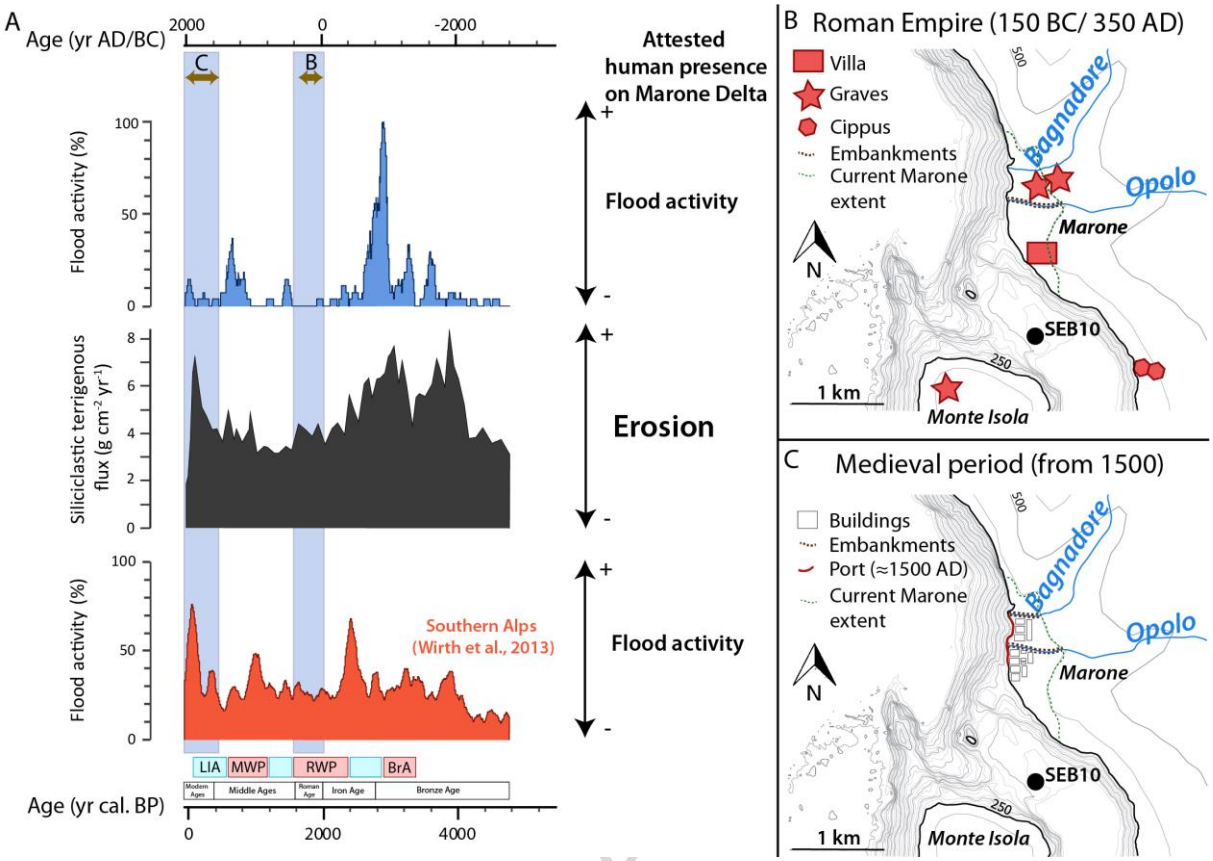

Figure 7 - (A) Comparison between SEB10 flood activity (calculated with the assumption that the highest frequency recorded correspond to 100 % of flood activity), the Southern Alps flood chronicle (Wirth et al., 2013) and the total solar irradiance (W.m²) curve (Steinhilber et al., 2012) from 4.8 kyr cal BP to the present. Light blue shading highlights periods of attested human presence on the Marone Delta. Blue and red boxes represent a period of attested cold/wet and warm/dry climate respectively. LIA: Little Ice Age; MWP: Medieval Warm Period; RWP: Roman Warm Period; BrA: Bronze Age Optimum (B) Sketch of the location of Roman archeological sites on the Marone delta (Condina, 1986) and supposed flow direction of the Opolo and Bagnadore streams during the Roman Empire Period (150 BC/ 350 AD). (C) Sketch of the Marone village during the Little Ice Age (from 1500 AD) and the location of attested embankments of the Bagnadore and Opolo streams (Gregorini et al., 2012).

Between 1.6 and 1.4 kyr cal BP (350–550 AD), the increase of flood activity recorded in the SEB10 sequence could be linked to the abandonment of Roman sites on the lake shores during the fall of the Roman Empire (**Fig. 7A**). If the stream banks are not maintained, avulsions could occur, and the streams could flow again in the southern part of the Marone delta, thus bringing sediment to the Monte Isola Plateau.

Another example of the human influence on the SEB10 flood chronicle is apparent when considering the flood activity during the Little Ice Age (LIA) and the Medieval Warm Period (MWP) (**Figs. 7A&C**). Indeed, the LIA is a colder and wetter period presenting high flood activity while the MWP is a drier and warmer period with low flood activity (**Fig. 7;** Sabatier et al., 2017; Vannière et al., 2013; Wirth et

al., 2013). However, the SEB10 flood chronicle shows the exact opposite, with high and low flood activity occurring during the MWP and the LIA, respectively. Therefore, the SCTF signal increases between 0.5 and 0.1 kyr cal BP, which confirms significant erosion in the watershed, probably due to a wetter climate or an increase of land use. This apparent paradox can be solved when considering human occupation dynamics. Indeed, during the MWP, the site of the current Marone village was abandoned, and local people settled on the surrounding hills (Predali, 2010), thus leaving the streams free to avulse. Inversely, during the LIA, the Marone village was created (**Fig. 7C**), the population increased and the necessity to dam the streams in the northern part of the Marone delta appeared around at least 377 yr cal BP (1573 AD) to favor the development of the manufacturing companies and to protect the city (Gregorini et al., 2012). Thus, from 400 yr cal BP, the possible sediment input is limited to the small gullies of Monte Isola and Sale Marasino, which explains the low activity that was recorded.

6. Conclusions

This study presents one of the first detailed and continuous flood chronicles spanning the last 12 kyr cal BP in Northern Italy. The flood frequency is low from 12 to 4.2 kyr cal BP, which is consistent with the warmer and drier climate condition of the Early and Mid-Holocene and with other regional flood records that were reconstructed from lake sediments. From 4.2 kyr cal BP, the terrigenous flux in Lake Iseo, which is followed from 3.8 kyr cal BP by the flood frequency, increased until 2.9 kyr cal BP, as previously described for the western Mediterranean region. This transition is interpreted as a nonlinear climate response to the orbital-driven gradual decrease in summer insolation at 60°N, which induced the development of extreme meso-scale precipitation events in the Mediterranean region (Magny et al., 2013). Three peaks of high flood activities were observed at 3.6, 3.3 and 2.9 kyr cal BP and probably correspond to short-term regional wetter conditions. However, if the chronicle is in phase with the regional climate conditions until 2 kyr cal BP, human impact should be considered to have been a flood-triggering mechanism since at least 3.6 kyr cal BP. Indeed, forest opening and land

use are documented in southern Alps from at least 4 kyr cal BP, and human presence on the watershed is expected to have influenced the flood frequency toward higher values during wetter periods until 2 kyr cal BP. From 2 kyr cal BP to the present, human activity in the watershed is proposed to be the main driver of the flood frequency that was recorded in Lake Iseo sediments. The two streams at the origin of the sediment inputs at the coring location were dammed on several occasions during the Roman Period (2 kyr cal BP), which directly prevented sediment input during flooding and, thus, explains the disappearance of flood deposits. From 2 kyr cal BP, the chronicle is, thus, highly dependent on the anthropization of the river banks. In this instance, this chronicle cannot be used as a proxy of the regional paleohydrology due to the human influences in the watershed that were observed from at least 2 kyr cal BP. The lack of an in-depth study of the evolution of human activities on the shores of Lake Iseo could have led to a misinterpretation of the flood activity. Thus, the use of a flood chronicle that is based on lake sediments to reconstruct past hydrological conditions should always be linked to a thorough study of the human activity in the watershed, even in a large lake and low elevation system.

Table 1

Sample Name	Core	MCD (cm)	Composite Depth(cm)	Radiocarbon age	Age cal yr BP 2 σ range	Sample type
SacA 25929	**SEB10-P1**	**21.5**	**21.5**	**165 ± 30**	**-3-288**	**wood**
SacA41380	SEB10-1A	170.5	149.3	1090 ± 30	938-1057	wood
SacA41381	SEB10-1B	239.5	206.1	1700 ± 30	1545-1696	wood
SacA 25937	SEB10-1B	323.6	281.9	2340 ± 30	2316-2455	wood
SacA41382	SEB10-1B	411.5	350.2	2900 ± 40	2926-3163	wood
SacA 25926	SEB10-1C	439.6	374.3	2890 ± 35	2899-3155	wood
SacA 25927	SEB10-1C	453.5	384.2	2945 ± 30	2999-3206	wood
SacA 25928	SEB10-1C	453.5	384.2	2975 ± 30	3009-3315	wood
SacA41387	SEB10-2B	486.4	409.0	3180 ± 30	3359-3454	charcoal
SacA 25936	SEB10-1C	512.3	432.1	3330 ± 30	3479-3636	wood
SacA 25934	SEB10-1C	548.6	463.5	3515 ± 35	3697-3881	wood
SacA 25935	SEB10-1C	612.5	523.3	3805 ± 35	4086-4380	wood

SacA41383	SEB10-1D	718.8	624.1	5090 ± 30	5749-5912	wood
SacA41389	SEB10-2D	745.8	648.9	5280 ± 30	5946-6180	wood
SacA41390	SEB10-2D	779.3	682.4	5805 ± 30	6504-6672	wood
SacA41384	**SEB10-1D**	**785.8**	**688.9**	**6120 ± 40**	**6905-7157**	**vivianite**
SacA 25932	SEB10-3A	786.6	689.4	5715 ± 40	6411-6630	wood
SacA 25930	SEB10-3B	854.4	755.3	6670 ± 40	7474-7606	wood
SacA41388	SEB10-2D	865.3	765.9	7090 ± 50	7829-8008	charcoal
SacA41391	**SEB10-2D**	**887.5**	**786.1**	**7630 ± 45**	**8374-8537**	**wood**
SacA 25939	SEB10-3B	897.7	796.3	7400 ± 45	8060-8347	wood
SacA41392	SEB10-2D	915.3	813.9	8090 ± 40	8787-9132	wood
SacA 25941	SEB10-2E	1060.0	955.5	10305 ± 50	11842-12386	wood
SacA 25933	SEB10-3C	1165.0	1060.5	11970 ± 60	13618-14023	wood
Ouverture 1	SEB10-3C	1165.5	1061.0	12040 ± 60	13752-14056	twig
SacA 25942	SEB10-2F	1188.7	1084.2	12520 ± 60	14354-15101	wood
SacA 25938	SEB10-2F	1266.5	1162.0	13440 ± 70	15932-16408	wood

Acknowledgments

We thank the Laboratoire Souterrain de Modane (France) for the gamma spectrometry measurements, the CNRS-INSU ARTEMIS national radiocarbon AMS measurement program at Laboratoire de Mesure du ^{14}C (LMC14) in the CEA Institute at Saclay (French Atomic Energy Commission) for ^{14}C measurements and EDYTEM (Environnement, Dynamique et Territoires de Montagne, France) for the X-ray fluorescence analyses. We are grateful to the Autorita' di bacino lacuale dei laghi d'Iseo, Endine e Moro for permission to core Lake Iseo. Daniel Arnaud (INSU, C2FN) helped with coring. Coring was funded by INSU (Institut National des sciences de l'Univers, CNRS, France) and CEA (Commissariat à l'Energie Atomique et aux Energies Alternatives) through ISOMEX/PALEOMEX. We thank Adrian Gilli for his participation in the 2007 seismic survey. We are also grateful to Ana Brancelj for her valuable help during the bibliographical work.

References

Anati, E., Cittadini, T., 1994. Valcamonica rock art: a new history for Europe.

Appleby, P.G., Richardson, N., Nolan, P.J., 1991. 241Am dating of lake sediments, in: Smith, J.P., Appleby, P.G., Battarbee, R.W., Dearing, J.A., Flower, R., Haworth, E.Y., Oldfield, F., O'Sullivan, P.E. (Eds.), Environmental History and Palaeolimnology, Developments in Hydrobiology. Springer Netherlands, pp. 35–42. https://doi.org/10.1007/978-94-011-3592-4_4

Arcà, A., Fossati, A., 2006. Rupestrian archaeology: a methodological approach to the rock engravings of Valcamonica. Eur. II Prehist. Art Res. Manag. Eur. Stud. Archeol. Storia Cult. 4, 51–8.

Arnaud, F., Lignier, V., Revel, M., Desmet, M., Beck, C., Pourchet, M., Charlet, F., Trentesaux, A., Tribovillard, N., 2002. Flood and earthquake disturbance of 210Pb geochronology (Lake Anterne, NW Alps). Terra Nova 14, 225–232. https://doi.org/10.1046/j.1365-3121.2002.00413.x

Arnaud, F., Poulenard, J., Giguet-Covex, C., Wilhelm, B., Révillon, S., Jenny, J.-P., Revel, M., Enters, D., Bajard, M., Fouinat, L., others, 2016. Erosion under climate and human pressures: An alpine lake sediment perspective. Quat. Sci. Rev. 152, 1–18.

Bajard, M., Poulenard, J., Sabatier, P., Develle, A.-L., Giguet-Covex, C., Jacob, J., Crouzet, C., David, F., Pignol, C., Arnaud, F., 2017a. Progressive and regressive soil evolution phases in the Anthropocene. Catena 150, 39–52.

Bajard, M., Poulenard, J., Sabatier, P., Etienne, D., Ficetola, F., Chen, W., Gielly, L., Taberlet, P., Develle, A.-L., Rey, P.-J., 2017b. Long-term changes in alpine pedogenetic processes: Effect of millennial agro-pastoralism activities (French-Italian Alps). Geoderma 306, 217–236.

Bajard, M., Sabatier, P., David, F., Develle, A.-L., Reyss, J.-L., Fanget, B., Malet, E., Arnaud, D., Augustin, L., Crouzet, C., Poulenard, J., Arnaud, F., 2016. Erosion record in Lake La Thuile sediments (Prealps, France): Evidence of montane landscape dynamics throughout the Holocene. The Holocene 26, 350–364. https://doi.org/10.1177/0959683615609750

Benedetti, R., Predali, R., 2013. Contro al cieco fiume: cronaca fotografica delle alluvioni di Marone, 11 luglio 1953, e di Vello, 9 luglio 1963. FdP.

Beniston, M., Stephenson, D.B., Christensen, O.B., Ferro, C.A., Frei, C., Goyette, S., Halsnaes, K., Holt, T., Jylhä, K., Koffi, B., 2007. Future extreme events in European climate: an exploration of regional climate model projections. Clim. Change 81, 71–95.

Bertrand, S., Hughen, K.A., Sepulveda, J., Pantoja, S., 2012. Geochemistry of surface sediments from the fjords of Northern Chilean Patagonia (44–47 S): spatial variability and implications for paleoclimate reconstructions. Geochim. Cosmochim. Acta 76, 125–146.

Bini, A., Corbari, D., Falletti, P., Fassina, M., Perotti, C.R., Piccin, A., 2007. Morphology and geological setting of Iseo Lake (Lombardy) through multibeam bathymetry and high-resolution seismic profiles. Swiss J. Geosci. 100, 23–40.

Blaauw, M., 2010. Methods and code for 'classical'age-modelling of radiocarbon sequences. Quat. Geochronol. 5, 512–518.

Bøe, A.-G., Dahl, S.O., Lie, Ø., Nesje, A., 2016. Holocene river floods in the upper Glomma catchment, southern Norway: a high-resolution multiproxy record from lacustrine sediments: The Holocene. https://doi.org/10.1191/0959683606hl940rp

Brisset, E., Guiter, F., Miramont, C., Troussier, T., Sabatier, P., Poher, Y., Cartier, R., Arnaud, F., Malet, E., Anthony, E.J., 2017. The overlooked human influence in historic and prehistoric floods in the European Alps. Geology 45, 347–350.

Bruel, R., Marchetto, A., Bernard, A., Lami, A., Sabatier, P., Frossard, V., Perga, M.-E., 2018. Seeking alternative stable states in a deep lake. Freshw. Biol. 63, 553–568.

Buffoli, G., 2014. Monte Guglielmo (Brescia): relazione tra le faglie e le vulcaniti triassiche del versante sud-occidentale.= Monte Guglielmo (Brescia): Relationship faults and Triassic volcanites of the south-western mountainside.

Condina, F.A., 1986. Carta archeologica della media e bassa Val Camonica: F. 34-Breno. Ed." Quaderni Camuni".

Cosandey, C., Andréassian, V., Martin, C., Didon-Lescot, J.-F., Lavabre, J., Folton, N., Mathys, N., Richard, D., 2005. The hydrological impact of the Mediterranean forest: a review of French research. J. Hydrol. 301, 235–249.

Czymzik, M., Brauer, A., Dulski, P., Plessen, B., Naumann, R., von Grafenstein, U., Scheffler, R., 2013. Orbital and solar forcing of shifts in Mid-to Late Holocene flood intensity from varved sediments of pre-alpine Lake Ammersee (southern Germany). Quat. Sci. Rev. 61, 96–110.

Dapples, F., Lotter, A.F., van Leeuwen, J.F., van der Knaap, W.O., Dimitriadis, S., Oswald, D., 2002. Paleolimnological evidence for increased landslide activity due to forest clearing and land-use since 3600 cal BP in the western Swiss Alps. J. Paleolimnol. 27, 239–248.

Elbaz-Poulichet, F., Sabatier, P., Dezileau, L., Freydier, R., 2014. Sedimentary record of V, U, Mo and Mn in the Pierre-Blanche lagoon (Southern France)–Evidence for a major anoxia event during the Roman period. The Holocene 24, 1384–1392.

Gaume, E., Bain, V., Bernardara, P., Newinger, O., Barbuc, M., Bateman, A., Blaškovičová, L., Blöschl, G., Borga, M., Dumitrescu, A., Daliakopoulos, I., Garcia, J., Irimescu, A., Kohnova, S., Koutroulis, A., Marchi, L., Matreata, S., Medina, V., Preciso, E., Sempere-Torres, D., Stancalie, G., Szolgay, J., Tsanis, I., Velasco, D., Viglione, A., 2009. A compilation of data on European flash floods. J. Hydrol. 367, 70–78. https://doi.org/10.1016/j.jhydrol.2008.12.028

Gehrig, R., 1997. Pollenanalytische Untersuchungen zur Vegetations-und-Klimageschichte des Val Camonica (Norditalien).

Giguet-Covex, C., Arnaud, F., Enters, D., Poulenard, J., Millet, L., Francus, P., David, F., Rey, P.-J., Wilhelm, B., Delannoy, J.-J., 2012. Frequency and intensity of high-altitude floods over the last 3.5 ka in northwestern French Alps (Lake Anterne). Quat. Res. 77, 12–22.

Gilli, A., Anselmetti, F.S., Glur, L., Wirth, S.B., 2013. Lake sediments as archives of recurrence rates and intensities of past flood events, in: Dating Torrential Processes on Fans and Cones. Springer, pp. 225–242.

Giorgi, F., Torma, C., Coppola, E., Ban, N., Schär, C., Somot, S., 2016. Enhanced summer convective rainfall at Alpine high elevations in response to climate warming. Nat. Geosci. 9, 584.

Glur, L., Wirth, S.B., Büntgen, U., Gilli, A., Haug, G.H., Schär, C., Beer, J., Anselmetti, F.S., 2013. Frequent floods in the European Alps coincide with cooler periods of the past 2500 years. Sci. Rep. 3, 2770.

Gregorini, G., Tacchini, G., Pennachio, M., Predali, R., 2012. L'economia bresciana di fronte all'Unità d'Italia. Il lanificio sebino. roberto predali.

Heiri, O., Lotter, A.F., Lemcke, G., 2001. Loss on ignition as a method for estimating organic and carbonate content in sediments: reproducibility and comparability of results. J. Paleolimnol. 25, 101–110.

Hirabayashi, Y., Mahendran, R., Koirala, S., Konoshima, L., Yamazaki, D., Watanabe, S., Kim, H., Kanae, S., 2013. Global flood risk under climate change. Nat. Clim. Change 3, 816.

Isola, I., Zanchetta, G., Drysdale, R.N., Regattieri, E., Bini, M., Bajo, P., Hellstrom, J.C., Baneschi, I., Lionello, P., Woodhead, J., 2019. The 4.2 ka event in the central Mediterranean: new data from a Corchia speleothem (Apuan Alps, central Italy). Clim. Past 15, 135–151.

Jenny, J.-P., Arnaud, F., Dorioz, J.-M., Covex, C.G., Frossard, V., Sabatier, P., Millet, L., Reyss, J.-L., Tachikawa, K., Bard, E., 2013. A spatiotemporal investigation of varved sediments highlights the dynamics of hypolimnetic hypoxia in a large hard-water lake over the last 150 years. Limnol. Oceanogr. 58, 1395–1408.

Joannin, S., Magny, M., Peyron, O., Vannière, B., Galop, D., 2014. Climate and land-use change during the late Holocene at Lake Ledro (southern Alps, Italy). The Holocene 24, 591–602.

Joannin, S., Vannière, B., Galop, D., Peyron, O., Haas, J.N., Gilli, A., Chapron, E., Wirth, S.B., Anselmetti, F.S., Desmet, M., 2013. Climate and vegetation changes during the Lateglacial and early-middle Holocene at Lake Ledro (southern Alps, Italy). Clim. Past 9, 913–933.

Lauterbach, S., Chapron, E., Brauer, A., Hüls, M., Gilli, A., Arnaud, F., Piccin, A., Nomade, J., Desmet, M., Von Grafenstein, U., 2012. A sedimentary record of Holocene surface runoff events and earthquake activity from Lake Iseo (Southern Alps, Italy). The Holocene 22, 749–760.

Magny, M., Combourieu-Nebout, N., De Beaulieu, J.L., Bout-Roumazeilles, V., Colombaroli, D., Desprat, S., Francke, A., Joannin, S., Ortu, E., Peyron, O., 2013. North-south palaeohydrological contrasts in the central Mediterranean during the Holocene: tentative synthesis and working hypotheses. Clim. Past 9, 2043–2071.

Magny, M., Galop, D., Bellintani, P., Desmet, M., Didier, J., Haas, J.N., Martinelli, N., Pedrotti, A., Scandolari, R., Stock, A., 2009. Late-Holocene climatic variability south of the Alps as recorded by lake-level fluctuations at Lake Ledro, Trentino, Italy. The Holocene 19, 575–589.

Magny, M., Joannin, S., Galop, D., Vannière, B., Haas, J.N., Bassetti, M., Bellintani, P., Scandolari, R., Desmet, M., 2012. Holocene palaeohydrological changes in the northern Mediterranean borderlands as reflected by the lake-level record of Lake Ledro, northeastern Italy. Quat. Res. 77, 382–396.

Moreno, A., Valero-Garcés, B.L., González-Sampériz, P., Rico, M., 2008. Flood response to rainfall variability during the last 2000 years inferred from the Taravilla Lake record (Central Iberian Range, Spain). J. Paleolimnol. 40, 943–961.

Nash, G., 2011. Replicating cultural landscapes: Interpreting rock-art in the Valcamonica, Lombardy, Italy. Landscapes 12, 1–19.

Nash, G., Chippindale, C., 2002. European landscapes of rock-art. Psychology Press.

Noren, A.J., Bierman, P.R., Steig, E.J., Lini, A., Southon, J., 2002. Millennial-scale storminess variability in the northeastern United States during the Holocene epoch. Nature 419, 821–824. https://doi.org/10.1038/nature01132

Pilotti, M., Valerio, G., Giardino, C., Bresciani, M., Chapra, S.C., 2018. Evidence from field measurements and satellite imaging of impact of Earth rotation on Lake Iseo chemistry. J. Gt. Lakes Res. 44, 14–25. https://doi.org/10.1016/j.jglr.2017.10.005

Pilotti, M., Valerio, G., Leoni, B., 2013. Data set for hydrodynamic lake model calibration: A deep prealpine case. Water Resour. Res. 49, 7159–7163.

Predali, R., 2013. I Ghitti di Bagnadore: Una famiglia, un paese. Marone tra 1500 e 1800. Roberto Predali.

Predali, R., 2010. La chiesa dei Santi Pietro e Paolo di Pregasso: storia, arte e tradizione. FdP Editore.

Predali, R., 2008. Marone tra 1500 e 1600: l'antica parrocchiale, FdP editore. ed. roberto predali.

Presbitero, M., Piccin, A., Cassinis, G., Perotti, C.R., Calabro', R.A., Vercesi, P.L., Falletti, P., Siletto, G.B., Jadoul, F., Bersezio, R., Schirolli, P., Ronchi, P., De Donatis, S., Bini, A., Corbari, D., Rigamonti, I., Besana, S., Dell'Orto, P., Gisolo, M., Cobianchi, N., Mancin, N., Ronchi, P., Cortesogno, L., Gaggero, L., Ivanova, D., Barbieri, P.M., Clerici, A., 2011. Foglio 099 : Iseo : Carta Geologica d'Italia alla scala 1:50000.

Reimer, P.J., Bard, E., Bayliss, A., Beck, J.W., Blackwell, P.G., Bronk Ramsey, C., Buck, C.E., Cheng, H., Edwards, R.L., Friedrich, M., others, 2013. IntCal13 and Marine13 radiocarbon age calibration curves 0-50,000 years cal BP.

Reyss, J.-L., Schmidt, S., Legeleux, F., Bonté, P., 1995. Large, low background well-type detectors for measurements of environmental radioactivity. Nucl. Instrum. Methods Phys. Res. Sect. Accel. Spectrometers Detect. Assoc. Equip. 357, 391–397.

Rottoli, M., Castiglioni, E., 2009. Prehistory of plant growing and collecting in northern Italy, based on seed remains from the early Neolithic to the Chalcolithic (c. 5600–2100 cal BC). Veg. Hist. Archaeobotany 18, 91–103.

Sabatier, P., Dezileau, L., Briqueu, L., Colin, C., Siani, G., 2010. Clay minerals and geochemistry record from northwest Mediterranean coastal lagoon sequence: Implications for paleostorm reconstruction. Sediment. Geol. 228, 205–217.

Sabatier, P., Wilhelm, B., Ficetola, G.F., Moiroux, F., Poulenard, J., Develle, A.-L., Bichet, A., Chen, W., Pignol, C., Reyss, J.-L., Gielly, L., Bajard, M., Perrette, Y., Malet, E., Taberlet, P., Arnaud, F., 2017. 6-kyr record of flood frequency and intensity in the western Mediterranean Alps –

Interplay of solar and temperature forcing. Quat. Sci. Rev. 170, 121–135. https://doi.org/10.1016/j.quascirev.2017.06.019

Steinhilber, F., Abreu, J.A., Beer, J., Brunner, I., Christl, M., Fischer, H., Heikkilä, U., Kubik, P.W., Mann, M., McCracken, K.G., 2012. 9,400 years of cosmic radiation and solar activity from ice cores and tree rings. Proc. Natl. Acad. Sci. 109, 5967–5971.

Stocker, T.F., Qin, D., Plattner, G.-K., Alexander, L.V., Allen, S.K., Bindoff, N.L., Bréon, F.-M., Church, J.A., Cubasch, U., Emori, S., 2013. Technical summary, in: Climate Change 2013: The Physical Science Basis. Contribution of Working Group I to the Fifth Assessment Report of the Intergovernmental Panel on Climate Change. Cambridge University Press, pp. 33–115.

Sturm, M., Matter, A., 1978. Turbidites and varves in Lake Brienz (Switzerland): deposition of clastic detritus by density currents. Wiley Online Library.

Swierczynski, T., Lauterbach, S., Dulski, P., Delgado, J., Merz, B., Brauer, A., 2013. Mid-to late Holocene flood frequency changes in the northeastern Alps as recorded in varved sediments of Lake Mondsee (Upper Austria). Quat. Sci. Rev. 80, 78–90.

Vannière, B., Magny, M., Joannin, S., Simonneau, A., Wirth, S.B., Hamann, Y., Chapron, E., Gilli, A., Desmet, M., Anselmetti, F.S., 2013. Orbital changes, variation in solar activity and increased anthropogenic activities: controls on the Holocene flood frequency in the Lake Ledro area, Northern Italy. Clim. Past 9, 1193–1209.

Wilhelm, B., Arnaud, F., Sabatier, P., Crouzet, C., Brisset, E., Chaumillon, E., Disnar, J.-R., Guiter, F., Malet, E., Reyss, J.-L., others, 2012. 1400years of extreme precipitation patterns over the Mediterranean French Alps and possible forcing mechanisms. Quat. Res. 78, 1–12.

Wilhelm, B., Arnaud, F., Sabatier, P., Magand, O., Chapron, E., Courp, T., Tachikawa, K., Fanget, B., Malet, E., Pignol, C., Bard, E., Delannoy, J.J., 2013. Palaeoflood activity and climate change over the last 1400 years recorded by lake sediments in the north-west European Alps. J. Quat. Sci. 28, 189–199. https://doi.org/10.1002/jqs.2609

Wirth, S.B., Glur, L., Gilli, A., Anselmetti, F.S., 2013. Holocene flood frequency across the Central Alps–solar forcing and evidence for variations in North Atlantic atmospheric circulation. Quat. Sci. Rev. 80, 112–128.

- In the Alps, flood frequency is higher during period of cold and wetter climate
- A major palaeohydrological transition is observed at approximately 4 kyr cal BP
- From 2 kyr cal BP, human activity is the main driver of the SEB10 flood frequency
- In Alpine lowland lake, flood chronicle can be impacted by the anthropization
- Studying human activity is needed for flood-paleohydrological reconstructions